Are the Hypo-Reflective Clumps Associated With Age-Related Macular Degeneration in Adaptive Optics Ophthalmoscopy Autofluorescent?

Ysé Borella,[1,2] Natalie Danielsen,[1,3] Evelyn M. Markle,[1] Valerie C. Snyder,[1] Daniel M. W. Lee,[1,3] Min Zhang,[1] Andrew W. Eller,[1] Jay Chhablani,[1] Michel Paques,[2] and Ethan A. Rossi[1,3,4]

[1]Department of Ophthalmology, University of Pittsburgh School of Medicine, Pittsburgh, Pennsylvania, United States
[2]Vision Institute, 15-20 National Ophthalmology Hospital, Clinical Investigation Center 1423 and Sorbonne University, Paris, France
[3]Department of Bioengineering, University of Pittsburgh Swanson School of Engineering, Pittsburgh, Pennsylvania, United States
[4]McGowan Institute for Regenerative Medicine, University of Pittsburgh, Pittsburgh, Pennsylvania, United States

Correspondence: Yse Borella, University of Pittsburgh School of Medicine, UPMC Vision Institute at Mercy Pavilion, Suite 8.396, 1622 Locust St., Pittsburgh, PA 15219, USA;
yse.borella@gmail.com.
Ethan A. Rossi, University of Pittsburgh School of Medicine, UPMC Vision Institute at Mercy Pavilion, Suite 8.396, 1622 Locust St., Pittsburgh, PA 15219, USA;
rossiea@pitt.edu.

YB and ND contributed equally to this work and should therefore be regarded as equivalent authors.

Received: May 31, 2024
Accepted: August 3, 2024
Published: August 21, 2024

Citation: Borella Y, Danielsen N, Markle EM, et al. Are the hypo-reflective clumps associated with age-related macular degeneration in adaptive optics ophthalmoscopy autofluorescent?. *Invest Ophthalmol Vis Sci.* 2024;65(10):28.
https://doi.org/10.1167/iovs.65.10.28

Purpose. Hypo-reflective clumps (HRCs) are structures associated with age-related macular degeneration (AMD) that were identified using flood-illumination adaptive optics ophthalmoscopy (FIAO) and hypothesized to be either macrophages that have accumulated melanin through the phagocytosis of retinal pigmented epithelial (RPE) cell organelles or transdifferentiated RPE cells. HRCs may be autofluorescent (AF) in the near infrared (NIR) but clinical NIR autofluorescence imaging lacks the resolution to answer this question definitively. Here, we used near infrared autofluorescence (NIRAF) imaging in fluorescence adaptive optics scanning laser ophthalmoscopy (AOSLO) to determine whether HRCs are AF.

Methods. Patients with AMD and HRCs underwent imaging with FIAO, optical coherence tomography (OCT), and multi-modal AOSLO (confocal, NIRAF, and non-confocal multi-offset detection using a fiber bundle). HRCs were segmented on FIAO and images, co-registered across modalities, and HRC morphometry and AF were quantified.

Results. Eight patients participated (mean age = 79 years, standard deviation [SD] = 5.7, range = 69–89 years, and 5 female patients). Most HRCs (86%, n = 153/178) were autofluorescent on AOSLO. HRC AF signal varied but most uniformly dark HRCs on FIAO showed corresponding AF on AOSLO, whereas heterogeneous HRCs showed a smaller AF area or no AF.

Conclusions. These findings are consistent with the hypothesis that HRCs contain AF RPE organelles. A small proportion of HRCs were not AF; these may represent macrophages that have not yet accumulated enough organelles to become AF. HRCs may have clinical significance but further study is needed to understand the interplay among HRCs, RPE cells, and macrophages, and their relationship to geographic atrophy (GA) progression in AMD.

Keywords: age-related macular degeneration (AMD), autofluorescence (AF), adaptive optics scanning light ophthalmoscopy (AOSLO), hypo-reflective clumps (HRCs), geographic atrophy (GA)

Age-related macular degeneration (AMD) is a major cause of blindness worldwide. Late-stage non-neovascular AMD is characterized by geographic atrophy (GA). GA represents complete outer retinal and retinal pigment epithelium (RPE) atrophy[1]; once GA is present, it usually relentlessly increases in size over time, although the rate of progression can vary substantially between patients. Adaptive optics ophthalmoscopy (AOO) allows for imaging of the living human retina with cellular level resolution. Flood-illumination adaptive optics ophthalmoscopy (FIAO) has shown microscopic dynamic structures that accompany the emergence and growth of GA. Longitudinal study has shown these hyporeflective clumps (HRCs),[2] as they have been termed in the literature, can dynamically change in number and size, and may disappear over time. HRCs are morphologically consistent with cells and have been hypothesized to be macrophages that have accumulated melanin through the phagocytosis of RPE organelles.[3] The inflammatory component of AMD is thought to be mediated in part through the activity of phagocytes and, if HRCs represent these cells, they may play an important role in the dynamics of GA progression. Thus, their morphology, activity, and

evolution may be useful for understanding disease status, risk for rapid progression, and possibly for evaluating response to treatment. Although GA is slowly progressing, these structures move rapidly,[2] potentially representing a biomarker of progression that can be evaluated over shorter timescales than the growth of GA lesions.

Melanin is an absorptive pigment that resides in RPE cells and is autofluorescent (AF) in the near infrared (NIR).[4] Previous work suggests that the near infrared autofluorescence (NIRAF) signal from the fundus in scanning laser ophthalmoscopy (SLO) mainly arises from melanin in RPE cells and that its excitation spectrum matches the absorption spectrum of melanin.[4] Melanolipofuscin, an aggregate of melanin and lipofuscin, also exhibits NIRAF; recent work has also suggested that lipofuscin itself can become AF in the NIR with aging, possibly through the incorporation of oxidated melanin species.[5] The dark appearance of HRCs in FIAO is suggestive of them containing an absorptive pigment, such as melanin. Gocho et al.[3] hypothesized that HRCs may be AF in the NIR, but conventional NIRAF imaging in commercial SLO could not answer this question definitively. However, fluorescence adaptive optics scanning light ophthalmoscopy (AOSLO) can image the microscopic distribution of NIRAF fluorophores with high precision.[6–8] Non confocal AOSLO imaging has also recently been shown to be capable of detecting presumed macrophages and microglia, providing an alternative mechanism to visualize presumed immune cells in the retina.[9] Here, we used high resolution imaging, including FIAO and multi-modal AOSLO with fluorescence and phase contrast multi-offset imaging to test the hypothesis that HRCs are AF in the NIR.

Methods

Eight patients with AMD with HRCs were recruited for imaging (mean age = 79 years, standard deviation [SD] = 5.7, range = 69–89, 5 female patients). Participants were patients with AMD that had previously shown HRCs on FIAO. We identified 11 eligible candidates with HRCs from a prior study (3–4 years earlier) that were contacted by phone and email. Of these, six agreed to be imaged, one declined participation, one had moved out of state, and three did not respond. Following imaging of these first six participants, two additional patients with AMD (cases 7 and 8) were recruited prospectively to increase the number of participants. Participants provided written informed consent prior to initiating study procedures. All aspects of the study were approved by the Institutional Review Board of the University of Pittsburgh prior to participant enrollment.

Each patient was imaged with infrared SLO (IR SLO), spectral domain optical coherence tomography (SD-OCT; Spectralis, Heidelberg Engineering), and FIAO (rtx1-e, Imagine Eyes, France) to determine AMD and HRC status followed by multi-modal AOSLO at preselected regions of interest (ROI) where HRCs were visible or where HRCs had been detected previously. FIAO montages were generated for all participants (images were registered using i2kRetina x64 Pro (DualAlign LLC, Clifton Park, NY, USA) using the following settings: (1) layout = quadratic; (2) blend = stack; and (3) aggressive registration = 10. These settings were used to generate a Photoshop document (PSD file) where the registered FIAO images were each on a separate layer without any automatic blending applied between overlapping images. This was done because the large differences in contrast and brightness that can be seen in patients with GA between adjacent imaging fields can often cause artifacts when using automatic blending. The hard edges at margins of overlap between adjacent images were then blended manually using the eraser tool in Adobe Photoshop (Adobe Systems Inc., San Jose, CA, USA). Finally, the brightness and contrast of some individual images were adjusted in Photoshop to provide relatively equal brightness and contrast across the final FIAO montages.

The AOSLO system used here is described in detail elsewhere.[6,10] In brief, it acquires 8 channels simultaneously at 30 frames per second. A 1-to-7 fan out custom optical fiber bundle with a small central fiber plus 6 radially arrayed offset fibers enabled simultaneous confocal and offset detection; airy disc diameters (ADDs) were 0.9 and 7.4, for the confocal and offset fibers, respectively. Illumination for confocal imaging and AF excitation was provided by a superluminescent diode (SLD) centered at 795 nm (full width at half maximum = 15 nm) for the first 6 cases. For cases 7 and 8, illumination was provided by a supercontinuum light source (SuperK Fianium FIR-20; NKT Photonics, Birkerød, Denmark) with attached tunable filter (VARIA) that allowed for selection of wavelength and bandwidth, center wavelength was 720 nm with 20 nm bandwidth. NIRAF emission for 795 nm excitation was collected from 814 to 850 nm and for 720 nm excitation was collected from 760 to 824 nm. Both configurations used the same confocal aperture (approximately 2.5 ADD) attached to a photomultiplier tube (PMT) mounted on a motorized translation stage for precise alignment, as described previously.[11] Confocal image sequences were registered using REMMIDE[12] and the computed motion offsets were applied to each of the other seven channels for co-registration. Images from each channel were then averaged to produce images for each of the confocal, AF, and six offset aperture channels. The orientation of each fiber was determined in a calibration phase and offset aperture images were fused using our previously published SMART[13] approach to generate fused phase contrast multi-offset images.

All putative HRCs were segmented manually and independently on the original individual FIAO images at each ROI by three graders (authors Y.B., N.D., and E.A.R.), that had no previous experience segmenting HRCs, using the pencil tool in Photoshop. These outlines were filled to create a binary image mask where the HRCs were shown in white and the background was black (see Supplementary Fig. S1, images in the left column). The three segmentation masks from each ROI were merged by summing them in Matlab (The MathWorks, Natick, MA, USA). The HRCs marked by at least two graders (portions in the sum map greater than or equal to 2) were then retained (see Supplementary Fig. S1, Merged) and a few small artifacts consisting of a few clusters of overlapping pixels were removed. The segmentation mask was then binarized (see Supplementary Fig. S1, Consensus) and the morphometric properties of each HRC were computed from it using the function "regionprops" in Matlab, including area, major axis, minor axis, diameter (mean of major and minor axis), and Feret's aspect ratio (major axis divided by minor axis). Results were expressed by mean and standard deviation (SD) and were graphically depicted by box and whisker plots or histograms. The ANOVA test was used to compare morphometric values between each case and multiple *t*-test was used if needed. Statistical analyses were performed using GraphPad Prism version 9. HRCs were determined to be AF if the AF level within the segmented HRC was over an arbitrary conserva-

Investigative Ophthalmology & Visual Science

tive threshold of 1.5 times the AF signal of the background; background signal for each ROI was defined by a user-selected ROI on each image. Pseudo-colored images were generated in Photoshop by assigning the AF image to the red and blue channels of an RGB image with the FIAO image assigned to the green channel.

Results

Of the eight patients imaged for this study (summarized in Table 1), six had definitive GA with visible HRCs (cases 1–5 and case 7), one had no visible HRCs (case 6), and one showed a few HRCs in an area that appeared to be transitioning to GA (case 8). FIAO montages of all 8 participants are provided as Supplementary Figures S2 to S9. Of the six cases with definitive GA, one had only a single HRC visible at the ROI imaged (case 4) and another had poor image quality on NIRAF AOSLO (case 5) so these were excluded from the morphometric analyses. This left five participants with multiple HRCs and sufficient image quality across all modalities for evaluation, four with GA and one transitioning to GA. The four patients with definitive GA had HRCs visible in areas of GA and in the transition zone around the GA (cases 1–3 and case 7; Figs. 1–3). HRCs in these participants were evaluated at five ROIs (including 2 ROIs from case 1; referred to as 1.1 and 1.2; see Figs. 1–3). HRCs had variable appearance across the AOO modalities (see Figs. 2C, 3). In FIAO (see Figs. 2C, 3A) and offset aperture AOSLO (see Fig. 3D), most HRCs appeared high contrast and were dark relative to the background. In confocal AOSLO (see Fig. 3B), HRCs had variable contrast and could appear either dark or bright, sometimes with an appearance suggestive of internal granularity (e.g. see Fig. 3.B.3). HRCs appeared relatively low contrast in non-confocal phase contrast AOSLO images (i.e. multi-offset modality images generated using SMART[13]; see Fig. 3E), with only the cell borders appearing visible on careful inspection. Interestingly, most HRCs that appeared dark on FIAO were co-localized with a hyper-AF signal on NIRAF AOSLO (highlighted as magenta on pseudo-colored images merging AF and FIAO in Fig. 3F).

HRCs were seen in an area appearing to be transitioning to GA in case 8 (Fig. 4). This participant showed signs on OCT suggesting disruption of the RPE layer on the margins of the area where HRCs were seen (see Figs. 4B–D).

Table 1. Demographic and Summary of ROI Data for All Participants Imaged

Case	Age, Y	Sex	Eye	Lens	ROIs (*n*)	ROI Structure	HRCs on FIAO?	Quantifiable NIRAF on AOSLO?	Included in Morphometric Analysis?
1	69	M	OS	1+ NS	2	GA	Yes	Yes	Yes
2	89	F	OS	IOL	1	GA	Yes	Yes	Yes
3	79	F	OD	IOL	1	GA	Yes	Yes	Yes
4	77	M	OD	2+ NS 2+ CS	1	GA	Yes	Yes	No
5	79	F	OS	IOL	1	GA	Yes	No	No
6	78	F	OD	2+ NS	1	Cicatricial lesion	No	Yes	No
7	79	F	OD	1+ NS 1+ CS	1	GA	Yes	Yes	Yes
8	84	M	OD	IOL	1	Thickened RPE transitioning to GA	Yes	Yes	Yes

CS, phakic with cortical spoking cataract; IOL, pseudophakic; *n*, number; NS, phakic with nuclear sclerotic cataract; ROI, region of interest.

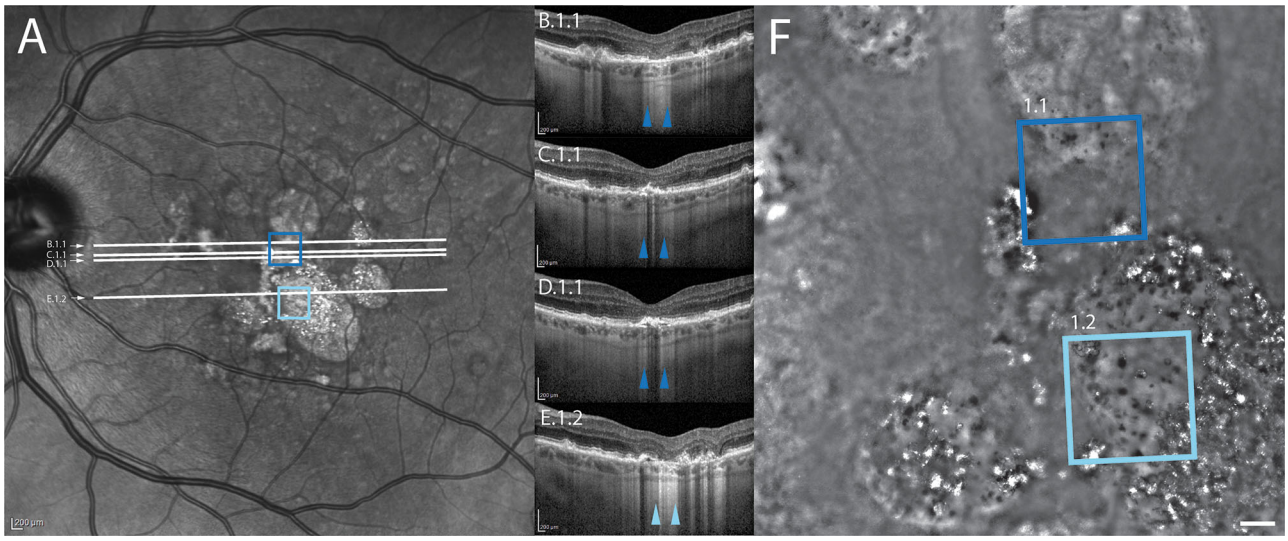

Figure 1. Clinical images for case 1. Squares on the infrared reflectance SLO (**A**) and flood-illumination adaptive optics images (**F**) denote the location of the ROIs shown in Figure 3. ROI 1.1 is denoted by the *dark blue square* and ROI 1.2 is denoted by the *light blue square*. *White lines* in (**A**) denote the position of the OCT b-scans shown in panels **B** to **E**. *Colored arrowheads* in **B** to **E** denote the margins of the ROI where it intersects the b-scans. Note that the multiple OCT sections for ROI 1.1 highlight different RPE layer aspects within the same ROI (GA in (**B**), disrupted RPE layer in (**C**), and thickened RPE in (**C**) and (**D**).

Investigative Ophthalmology & Visual Science

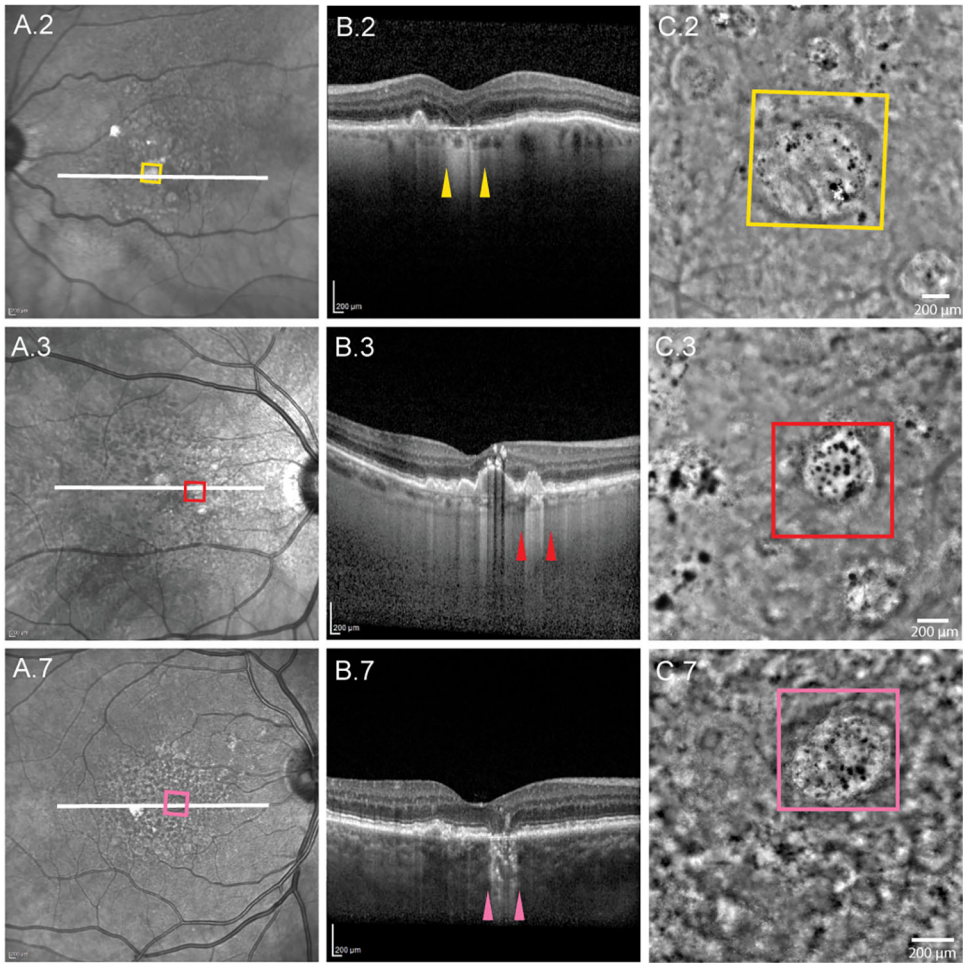

Figure 2. Clinical and FIAO images for cases 2 (*yellow*), 3 (*red*), and 7 (*pink*). *Colored squares* on the infrared reflectance SLO (**A**) and flood-illumination adaptive optics images (**C**) denote the location of the ROIs shown in Figure 3. *White lines* in (**A**) denote the positions of the OCT b-scans shown in (**B**). *Colored arrowheads* in (**B**) denote the margins of the ROIs where they intersect the b-scans.

However, in the central region the OCT showed thickening of the outer retinal bands (see Fig. 4C). Across the corresponding area on FIAO and AOSLO, this participant showed several structures that were morphologically consistent with HRCs but only a few of them were actually hyporeflective in FIAO (see Fig. 4E). Nearly all of them had a granular appearance on confocal AOSLO (see Fig. 4F) and all were AF on AOSLO (see Fig. 4G). Consistent with the definitive GA cases, the offset aperture images were similar to FIAO (see Fig. 4H). Nonconfocal phase contrast images could more clearly delineate the boundaries between adjacent structures (see Fig. 4I).

Across all 6 ROIs examined in the patients with HRCs, 86% of the segmented HRCs (153/178) were AF (see Table 2). Figures 5A and 5B show box-and-whiskers plots of HRC diameter and Feret's aspect ratio for the different ROIs. The distribution of HRC area across all HRCs is plotted in the histogram in Figure 5C. Table 1 lists the values for the additional summary statistics for each morphometric parameter assessed, as well as the *P* values from the statistical tests performed; differences between the means of the various morphological characteristics computed across the different ROIs were not statistically significant, aside from HRC diameter (see Table 2). Additional multiple pairwise *t*-tests exhibited a difference among case 2 and cases 1.2, 3, and 7 (see Table 2). The mean Feret's aspect ratio of all the HRCs was 1.4 (SD = 0.4) and ranged from 0.9 to 1.6 between the different ROIs.

In case 6, prior timelapse FIAO (Fig. 6A) and SD-OCT (Fig. 6B) showed that this ROI began as a drusen devoid of RPE but covered with several HRCs (see Fig. 6A). However, no HRCs were visible at the most recent follow-up with multi-modal AOO imaging (T = 39 months; see Figs. 6A–C). Instead, we observed collapse of the drusen and an aspect of cicatricial lesion with multiple cell-like structures in the vicinity of where HRCs had been seen previously which did not resemble HRCs and were not visible on FIAO but only detected on multi-modal AOSLO (see Fig. 6C). These structures did not resemble those seen in the other patients in this study. Due to their small size and limited number, we did not attempt to segment these structures and systematically quantify them. On multi-modal AOSLO, these structures exhibited variable contrast on confocal imaging (see Fig. 6C1), relatively high contrast on offset (see Fig. 6C3) and nonconfocal phase contrast AOSLO (see Fig. 6C4) and a low AF signal (see Fig. 6C2), which made it difficult to discern whether any of the individual structures exhibited NIRAF. Manual measurements on a few of the largest and smallest ones made using the measurement tool in Adobe Photoshop showed that most were in the range from 5 to 10 µm in diam-

Investigative Ophthalmology & Visual Science

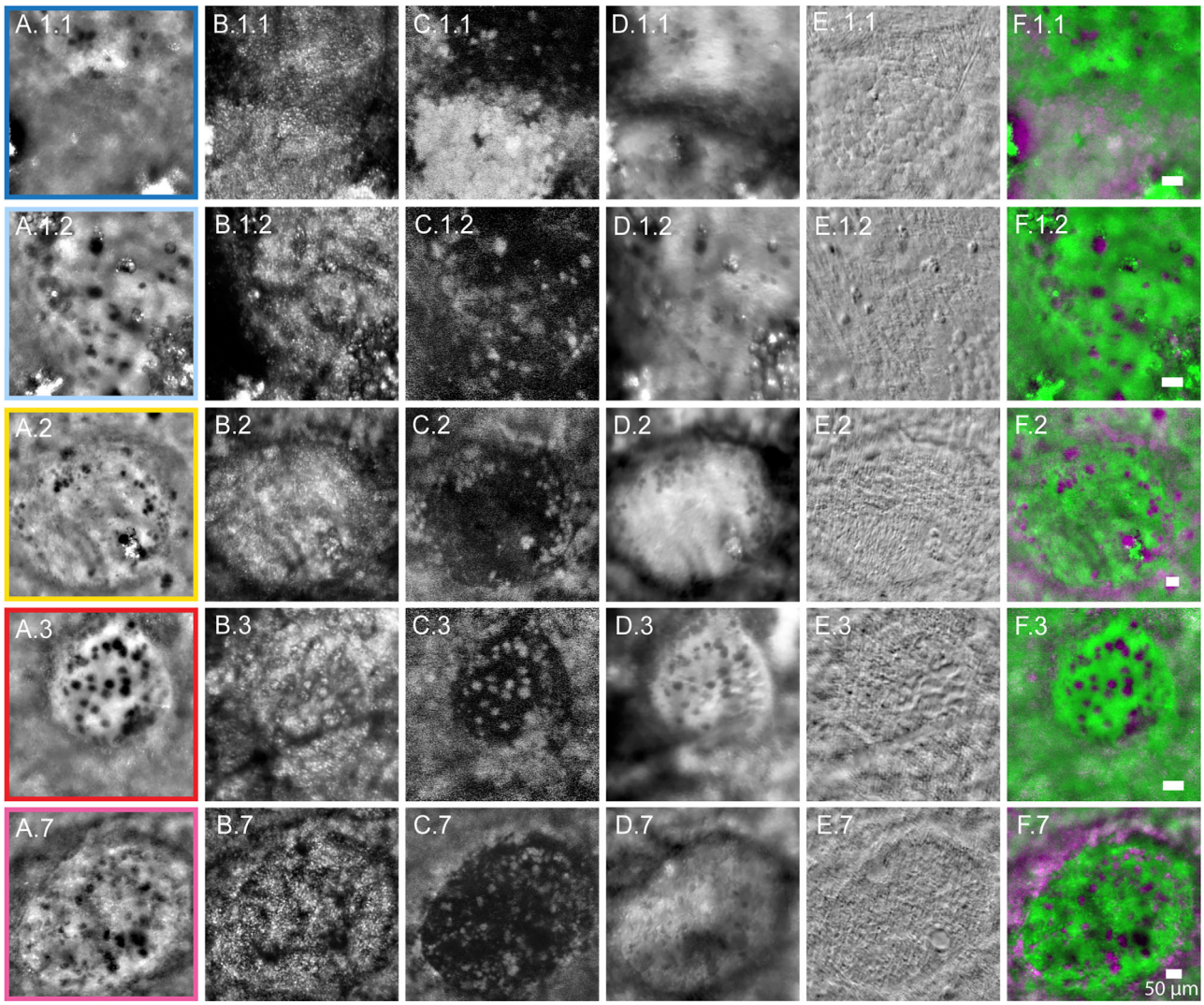

Figure 3. Corresponding FIAO and AOSLO images for case 1 ROIs 1.1 (*light blue*) and 1.2 (*dark blue*), case 2 (*yellow*), case 3 (*red*), and case 7 (*pink*). (**A**) FIAO and (**B**) confocal. (**C**) NIRAF. (**D**) Offset aperture. (**E**) Nonconfocal multi-offset phase contrast (SMART) AOSLO. (**F**) Merge images showing FIAO (pseudo colored in *green*) and NIRAF AOSLO (pseudo colored in *magenta*), highlighting autofluorescent HRCs in saturated *magenta*.

eter (e.g. see Fig. 6C, lower dark green arrow), with only one larger circular structure that was approximately 15 µm in diameter (see Fig. 6C, upper light green arrow).

Discussion

The finding that most HRCs exhibit NIRAF on AOSLO is consistent with the hypothesis that they contain AF organelles, most likely melanin and melanolipofuscin and possibly also oxidized melanin incorporated into lipofuscin.[5] Healthy RPE shows a decrease in melanin with age, possibly by photooxidation with aging.[14] A few studies have reported that melanin in young eyes may not be NIRAF but that the effect of photooxidation may render it NIRAF. This is of particular interest as NIRAF increases with age[15] and also particularly on the border of GA in AMD.[16] However, recent work from histology suggests that the source of NIRAF may not be as clear-cut as previously thought and that both melanin and lipofuscin may be AF in the NIR in older eyes.[5] Thus, the content of HRCs may be a mix of melanin, melanolipofuscin, and/or oxidized melanin incorporated into lipofuscin and linked to aging and oxidative stress.[5] Whether NIRAF signal could arise from molecules other than melanin-derived fluorophores would require chemical analysis of the content of the HRCs, something that should be pursued in a future study. NIRAF is being utilized more frequently in the evaluation of AMD, and is at least as, if not more, informative than blue autofluorescence (BAF),[17–20] therefore understanding its microscopic underpinnings is becoming increasingly important. It has been recently shown that pigment (melanin) dynamics on the margin of GA lesions could parallel GA progression,[21] so studying HRCs, containing melanin, could help to better understand GA dynamics.

The primary limitation of the present study is the small number of participants. GA has historically been difficult to image with AOSLO and the few previous reports in the literature also have small numbers of participants.[22–24] Older eyes have smaller pupils,[25–27] reducing the improvements that may be afforded by adaptive optic (AO) correction compared to larger pupils. Many also have cataracts

Investigative Ophthalmology & Visual Science

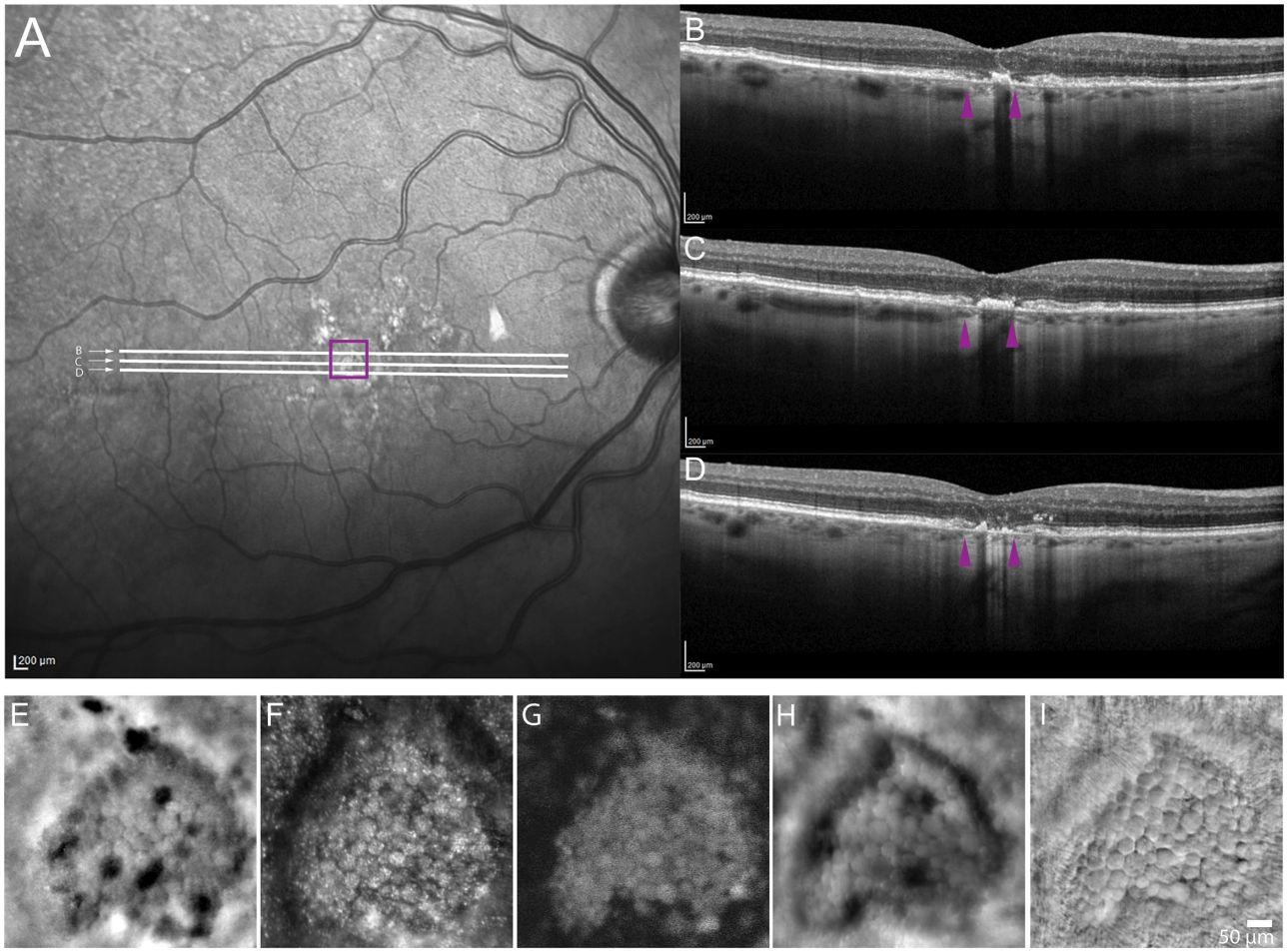

Figure 4. Case 8 showing an ROI that appears to be transitioning to GA. Square on the infrared reflectance SLO image (**A**) denotes the location of the ROI shown in (**E–I**). *White lines* in (**A**) denote location of OCT b-scans shown in (**B, C, D**) that show thickened outer retinal layers and disrupted RPE layer. *Purple arrowheads* in (**B, C, D**) denote the margins of the ROI where it intersects the b-scan. FIAO (**E**) and confocal (**F**), AF (**G**), offset aperture (**H**), and nonconfocal phase contrast SMART AOSLO (**I**), reveal structures consistent with HRCs. However, most were not hyporeflective on FIAO (**E**) and all appeared to be autofluorescent in NIR (**G**).

Table 2. Summary Statistics of HRC Morphometry for Each ROI

Case ROI	HRCs (*n*)	AF HRCs (*n*) (%)	Area-Mean (SD) (µm^2)	Area-Median (µm^2)	Diameter-Mean (SD) (µm)	Major Axis-Mean (SD) (µm)	Minor Axis-Mean (SD) (µm)	Feret's Aspect Ratio (SD)
Case 1.1	17	17 (100)	645.1 (425.8)	474.6	28.8 (9.8)	34.2 (11.8)	23.3 (8.5)	1.6 (0.5)
Case 1.2	12	10 (83)	358.3 (183)	361.9	21.6 (5.7)	26.4 (6.6)	16.8 (5.0)	1.6 (0.3)
Case 2	63	46 (73)	743.5 (846.9)	477.5	27.1 (13.3)	34.8 (20.4)	22.9 (12.4)	0.9 (0.5)
Case 3	30	27 (90)	589.3 (737.9)	391.7	27.8 (15.0)	30.6 (15.7)	21.9 (9.7)	1.3 (0.3)
Case 7	37	35 (95)	621.9 (407.3)	499.1	28.2 (9.4)	33.5 (12.7)	22.8 (7.3)	1.5 (0.3)
Case 8	19	19 (100)	765.1 (577.8)	494.0	31.1 (12.9)	37.4 (18.9)	24.7 (9.5)	1.5 (0.6)
P value	—	—	0.44	—	0.0003	0.48	0.40	0.29
All HRCs	178	154 (86.5)	514.3 (529.7)	476.05	27.4 (11.0)	32.8 (14.4)	22.1 (8.7)	1.4 (0.4)

n, number; ROI, region of interest; SD, standard deviation.

or intraocular lenses (IOLs); cataracts increase ocular scatter and decrease light throughput, whereas IOLs can limit the clear aperture for imaging and AO correction. Half of the patients in the present study had IOLs (including the one case who did not give quantifiable images on NIRAF AOSLO), whereas the other half had some level of cataract present (see Table 1). Many patients with GA also have poor fixation, especially when the GA involves the fovea, and this can present challenges for obtaining a sufficient number of frames for averaging, especially when considering that AF imaging requires hundreds of frames to be averaged to generate a high signal to noise ratio image.[6,7,11,28] All participants included here had GA with foveal sparing to ensure stable fixation, however, it has been reported recently that

Investigative Ophthalmology & Visual Science

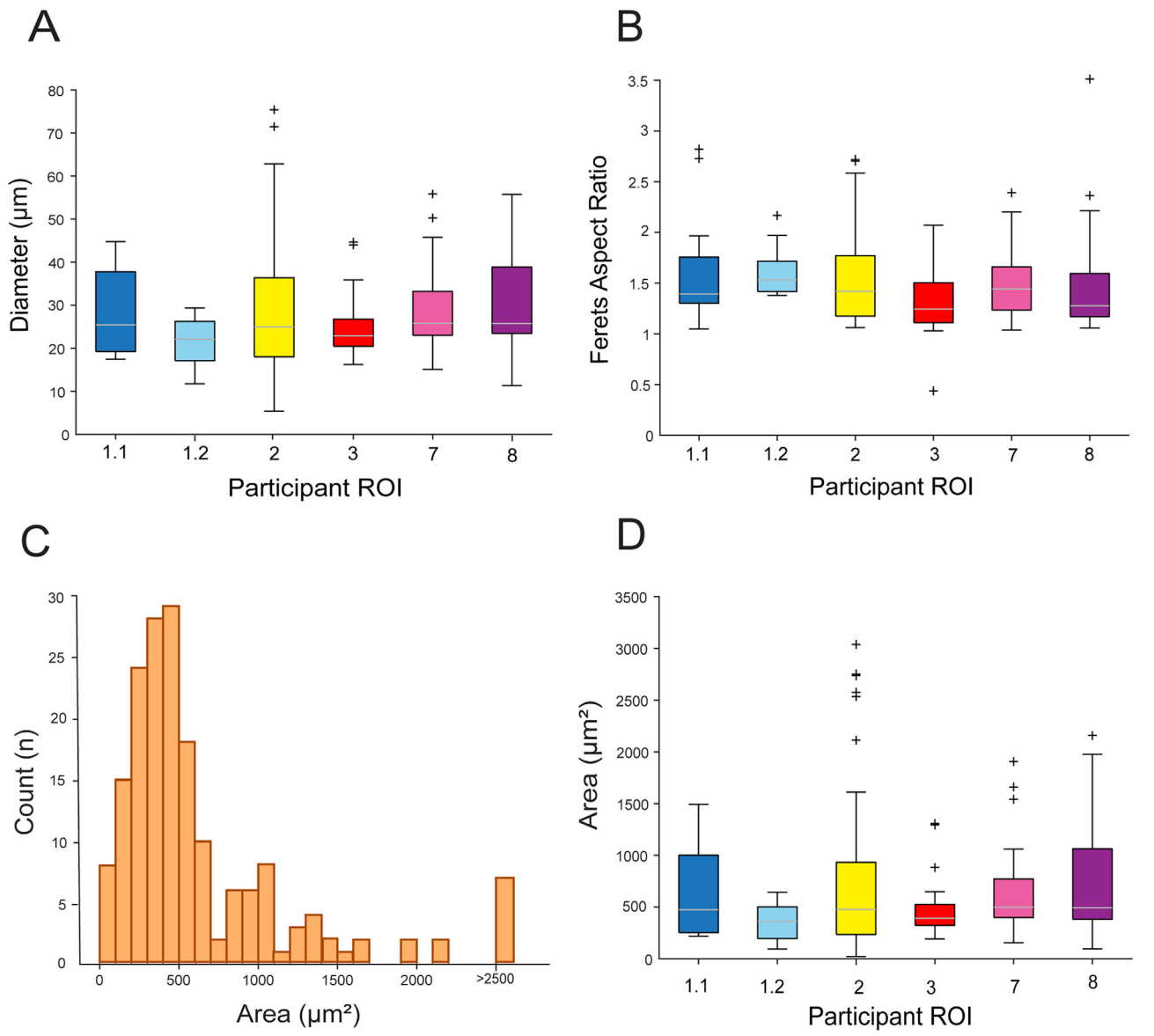

Figure 5. HRCs AF and morphological characteristics for each participant ROI. Boxplots show HRCs diameter (**A**), Feret's aspect ratio (**B**), and HRC area (**D**). On each box, the central mark indicates the median, and the bottom and top edges the 25th and 75th percentiles, respectively; whiskers extend to the most extreme data points not considered outliers, and the outliers are plotted using individual symbols. (**C**) Histogram of HRCs area. We hypothesize that the relatively normal distribution seen for HRCs with areas less than 750 µm^2 correspond to single HRCs, whereas those greater than 750 µm^2 represent clusters of 2 or more HRCs that were segmented as one.

even small foveolar drusen can decrease fixation stability.[29] GA tends to be challenging to image in AOSLO even when fixation is normal, particularly at its margins, because there is usually a large difference in thickness and retinal reflectivity between areas of GA and the transition zone around the GA. Even normal fixational eye motion can make the AO correction unstable at the margin of GA as the closed-loop AO correction can be driven to different focal planes depending on the light reaching the wavefront sensor as the eye moves between these large differences in reflectivity and retinal thickness. Another challenge is that GA presents differently in all patients, making it difficult to standardize the imaging protocol to, for example, image all participants in the same region or at the same retinal eccentricity. Future studies should evaluate the AF and evolution of HRCs in a larger cohort and in a longitudinal study. These investigations could be facilitated through multi-centric studies, improved eye tracking, and by increasing the detection efficiency of NIRAF AOSLO.

Additional limitations of the present study include the use of manual segmentation of the HRCs for quantitative analysis and the use of an arbitrary relative AF level selected manually for determining the AF status of the HRCs. Improvements required for future study should include the development of automatic, objective methods for HRC segmentation and AF quantification. An automated background AF quantification would be valuable for objectively determining AF status. Quantitative NIRAF measurements could also provide a more objective method for determining the AF status of HRCs and their evolution in a longi-

Investigative Ophthalmology & Visual Science

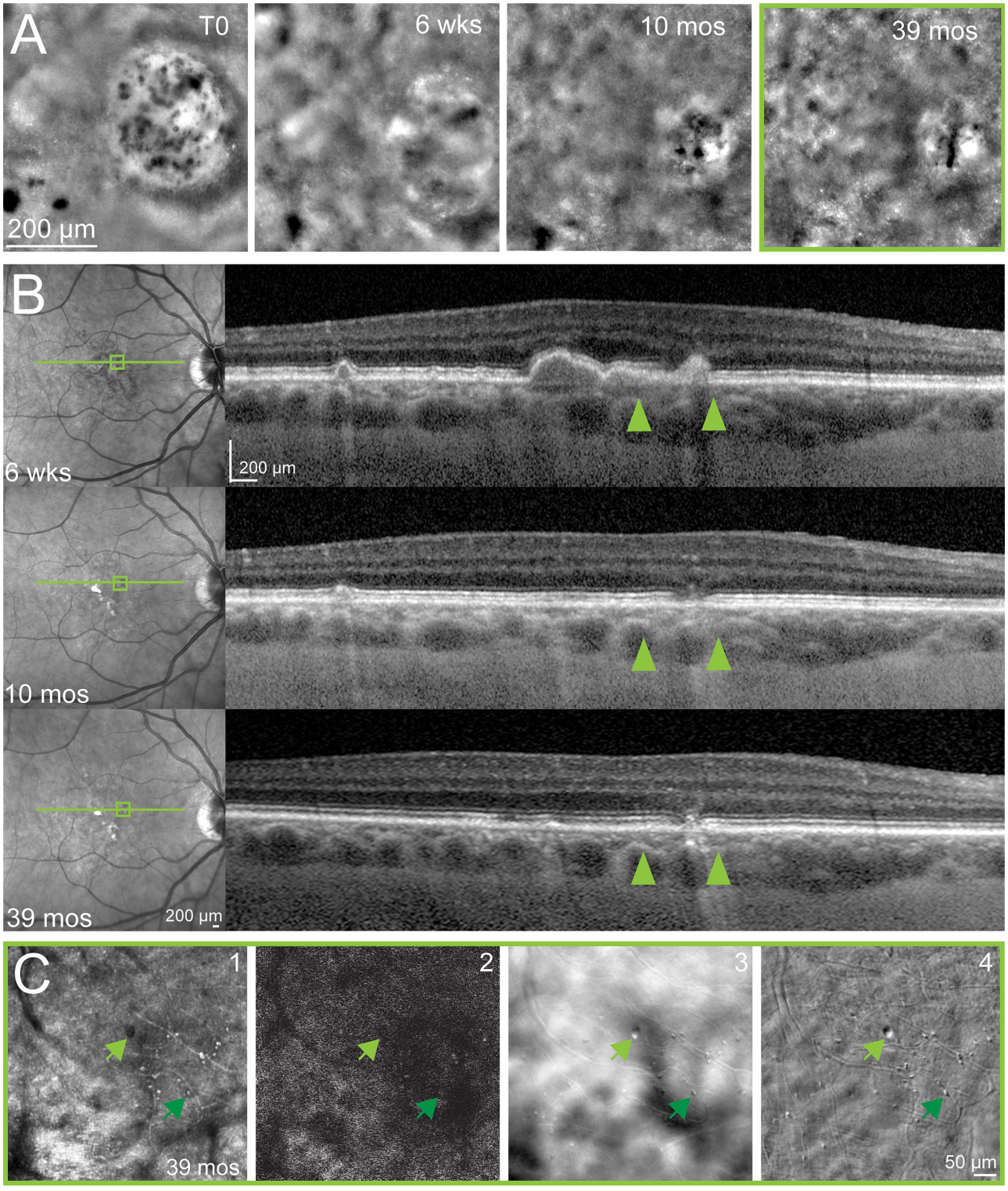

Figure 6. Case 6. Disappearance of HRCs across time in one patient. (**A**) HRCs were seen on FIAO imaging at T0, then FIAO imaging took place at time points of 6 weeks, 10 months and 39 months later. (**B**) Corresponding available SLO and SD-OCT for time points of 6 weeks (drusenoid deposit), 10 months (disappearance of the drusenoid deposit and what we hypothesized to be the beginning of GA), and 39 months (aspect of cicatricial RPE/ellipsoid zone). For T0, no corresponding OCT was taken at that time, however, we hypothesized it to be over a drusen, based on the OCT from 6 weeks. (**C**) AOSLO at the 39-month time point revealed multiple objects on confocal (1), offset (3), and multi-offsets images (4), denoted by *green arrowheads* that were not NIRAF (2). *Upper light green arrow* denotes the largest structure detected (approximately 15 µm in diameter). *Lower dark green arrow* shows an example of one of the several smaller objects seen on AOSLO.

Investigative Ophthalmology & Visual Science

tudinal study. A future longitudinal study will allow us to better understand the origin, composition, and evolution of HRCs as well as their relationship to GA progression in AMD.

HRCs on confocal AOSLO appeared relatively hyporeflective but were not as uniformly dark or as high contrast as they appear in FIAO, often showing some granularity. This may in part be due to the image processing applied to FIAO images from the internal software of the machine, which tends to saturate at the highest and lowest intensity levels; FIAO also has poorer lateral resolution than AOSLO. HRCs were usually hyporeflective and high contrast on offset aperture AOSLO, similar to their appearance in FIAO. This is not surprising considering that the lack of confocal gating in FIAO allows it to collect the multiply scattered light that is detected in the offset aperture modality of AOSLO. When offset aperture images were combined to minimize absorptive contrast and enhance phase contrast using our SMART image combination approach,[13] most HRCs appeared to be low contrast. Taken together, these properties suggest that most HRCs contain absorptive material, consistent with the hypothesis that they contain melanin.

Morphological analyses revealed that HRCs were similar in diameter across patients, on average, with a mean diameter of 27.4 µm (range = 21.6−31.1 µm). This is consistent with a previous report on HRCs,[3] the size of microglia,[30] mononuclear phagocytes,[31] and also the "transdifferentiated RPE cells"[32] that have been observed in histological samples of GA. Interestingly, the average sizes we observed for the HRCs are near what previous publications have deemed to be a cut-off point for the hyper-reflective foci (HRF) that have been detected previously in inflammatory conditions, such as AMD and diabetic retinopathy, on SD-OCT.[33] Future study is required to better understand the differences between HRCs and HRF and any potential overlap between these entities. Feret's aspect ratio analysis revealed HRCs to be elliptical in shape, on average (see Fig. 5B). The distribution of measured HRC areas (see Fig. 5C) follows a relatively normal distribution for HRCs less than about 750 µm^2, peaking between 400 and 500 µm^2; we hypothesize that this most likely corresponds to the distribution of areas for individual HRCs. The small number of HRCs detected with larger areas likely represent multiple HRCs that were segmented as one due to them overlapping and not appearing distinct as individual structures. This is not surprising, due to the relatively poor axial resolution of FIAO and AOSLO and the possibility that HRCs can aggregate together into larger clusters. We suspect that these clusters of overlapping HRCs are what resulted in statistical testing suggesting a difference in the diameter of HRCs across participants despite the mean diameters being quite similar across eyes. However, this potential for these structures to appear as clustered aggregates does present some challenges for accurate segmentation and morphometric analyses of individual HRCs. Recently, transscleral illumination in FIAO has been demonstrated and it appears to delineate the RPE cells due to their pigmented content,[34] so may allow for more accurate segmentation and quantification of HRC aggregates and clusters in future study. Overall, the morphometric analysis of the HRCs we segmented here was consistent with cell morphologies and characteristics found in histology of GA of human eyes. However, many hypotheses are still ongoing regarding the nature of those cells, all of them implicating RPE cells because of the presence of melanin in them; among them macrophages phagocytosing RPE debris,[35] detached RPE cells,[36] other cell types, such as microglia,[37] or RPE cells undergoing epithelial mesenchymal transition ("transdifferentiating cells").[32]

Although most HRCs were AF, there were some HRCs that did not exhibit NIRAF. However, careful inspection of these HRCs shows that the majority of them did not appear to be uniformly hyporeflective in FIAO and offset aperture AOSLO. This suggests that these structures may be distinct from the HRCs, either in their content or in their stage of development, which may be linked. It is possible that these structures represent macrophages that have not yet accumulated enough RPE organelles to become NIRAF. A longitudinal study that observed these structures becoming AF over time could bolster the hypothesis that HRCs represent phagocytes or macrophages rather than transdifferentiated RPE cells that should presumably be consistently NIRAF throughout their lifecycle.

Case 8 may provide some insight into the early evolution of HRCs in the time course of GA, as we hypothesize that the ROI examined is either an area of incomplete outer retinal atrophy (iRORA)[38] that is undergoing transition to GA or an area of thickened RPE (tRPE).[39] The confluent AF structures seen in this case on AOSLO were similar to those seen on ROI 1.1 (compare Fig. 4G to Fig. 3C1.1). Interestingly, in that example, none of those AF structures were hyporeflective, whereas only a few were in case 8. It is possible that this shared morphology between these two ROIs may reflect a similar stage of the degenerative process. The structures seen in this area are similar between the two ROIs. Measurements of several of the smallest and largest ones in case 8 (see Figs. 4E–I) show that they range in diameter from approximately 18 to 60 µm; assuming that they are hexagonal, this would correspond to an area of 210 to 2300 µm^2. Based on the measurements in the literature for RPE cell area at this eccentricity (near the foveal center)[7,40] we would expect normal RPE cell area to range from approximately 100 to 200 µm^2, meaning that the smallest cells in these ROIs are close to what would be expected for normal RPE cells but that the largest ones are much larger than the range expected for normal RPE cells. The morphological appearance of these structures on confocal and phase contrast AOSLO in both cases are also similar to those shown in a recent report from a case of Stargardt's disease,[41] suggesting that these outer retinal degenerations may share similar mechanistic underpinnings. Interestingly, in that patient with Stargardt's disease, the lesion appeared hyper-AF on short wavelength clinical fundus autofluorescence imaging, although that study lacked NIRAF and high resolution AF on AOSLO making it difficult to directly compare the AF findings.[41] Follow-up imaging may help us better understand the role and behavior of the NIRAF structures observed at the fovea in this patient in the progression from pathologic RPE (iRORA or tRPE) to GA.

The observation in case 6 of the disappearance of the HRCs over time (see Fig. 6) demonstrates that future study must evaluate HRCs in timelapse imaging to study their evolution and relationship to progression. The small sample size here prevents us from making any grand conclusions regarding the patient whose GA did not appear to progress and whose HRCs disappeared over time. However, the appearance of the smaller, morphologically distinct, high phase contrast structures that reside where the HRCs had been previously is strikingly similar to the structures that we have observed previously using phase contrast multi-offset AOSLO in patients with posterior uveitis.[9] These structures

may represent immune cells (microglia or macrophages) and/or the sequelae of sustained inflammation. Longitudinal imaging in a larger cohort of patients is required to determine whether this patient represents an extremely rare outcome or if this pattern of progression, suggestive of an adaptive wound-healing response, can be seen in other patients. However, it is interesting to consider the possibility that some differences between patients in their genetics, environment, and/or immune response could lead to outcomes where the GA seems to halt in its progression. Determining the mechanisms underlying this phenomenon may provide pathways toward future treatments to halt GA progression.

Conclusions

Most HRCs are absorptive structures that are AF in the NIR, most likely due to them containing melanin, melanolipofuscin, and/or oxidized melanin. Tracking HRCs across time may help us to better understand their behavior and the relations among RPE, macrophages, and GA evolution. Correlation between the characteristics of HRCs and the progression of GA may help to decipher their role in the progression of the disease. This study has potential clinical relevance as we expect to be able to use the characteristics of HRCs to track the natural history of GA, and, more importantly, monitor the efficacy of medications designed to treat it.

Acknowledgments

Supported by Foundation Fighting Blindness PPA-0819-0772-INSERM, NIH Grant R01EY030517, NIH CORE Grant EY08098, the Eye and Ear Foundation of Pittsburgh, an unrestricted grant to the University of Pittsburgh Department of Ophthalmology from Research to Prevent Blindness, a PhD grant from Fondation pour la Recherche Medicale (FDM202106013565), and a medical scholarship from Edmond de Rothschild Foundation.

Disclosure: **Y. Borella**, None; **N. Danielsen**, None; **E.M. Markle**, None; **V.C. Snyder**, None; **D.M.W. Lee**, None; **M. Zhang**, None; **A.W. Eller**, None; **J. Chhablani**, None; **M. Paques**, None; **E.A. Rossi**, is an inventor on patents related to some aspects of the technologies used to carry out these experiments that are owned by the University of Rochester (US10,772,496; US10,123,697; and US10,092,181)

References

1. Wu Z, Pfau M, Blodi BA, et al. OCT signs of early atrophy in age-related macular degeneration: interreader agreement: classification of atrophy meetings report 6. *Ophthalmol Retina*. 2022;6(1):4–14.
2. Paques M, Meimon S, Rossant F, et al. Adaptive optics ophthalmoscopy: application to age-related macular degeneration and vascular diseases. *Prog Retin Eye Res*. 2018;66:1–16.
3. Gocho K, Sarda V, Falah S, et al. Adaptive optics imaging of geographic atrophy. *Invest Ophthalmol Vis Sci*. 2013;54(5):3673–3680.
4. Keilhauer CN, Delori FC. Near-infrared autofluorescence imaging of the fundus: visualization of ocular melanin. *Invest Ophthalmol Vis Sci*. 2006;47(8):3556–3564.
5. Taubitz T, Fang Y, Biesemeier A, Julien-Schraermeyer S, Schraermeyer U. Age, lipofuscin and melanin oxidation affect fundus near-infrared autofluorescence. *EBioMedicine*. 2019;48:592–604.
6. Vienola KV, Zhang M, Snyder VC, Sahel JA, Dansingani KK, Rossi EA. Microstructure of the retinal pigment epithelium near-infrared autofluorescence in healthy young eyes and in patients with AMD. *Sci Rep*. 2020;10(1):9561.
7. Granger CE, Yang Q, Song H, et al. Human retinal pigment epithelium: in vivo cell morphometry, multispectral autofluorescence, and relationship to cone mosaic. *Invest Ophthalmol Vis Sci*. 2018;59(15):5705–5716.
8. Liu T, Jung H, Liu J, Droettboom M, Tam J. Noninvasive near infrared autofluorescence imaging of retinal pigment epithelial cells in the human retina using adaptive optics. *Biomed Opt Express*. 2017;8(10):4348–4360.
9. Rui Y, Zhang M, Lee DMW, et al. Label-free imaging of inflammation at the level of single cells in the living human eye. *Ophthalmol Sci*. 2024;4(5):100475.
10. Gofas-Salas E, Rui Y, Mecê P, et al. Design of a radial multi-offset detection pattern for in vivo phase contrast imaging of the inner retina in humans. *Biomed Opt Express*. 2022;13(1):117–132.
11. Rossi EA, Rangel-Fonseca P, Parkins K, et al. In vivo imaging of retinal pigment epithelium cells in age related macular degeneration. *Biomed Opt Express*. 2013;4(11):2527–2539.
12. Zhang M, Gofas-Salas E, Leonard BT, et al. Strip-based digital image registration for distortion minimization and robust eye motion measurement from scanned ophthalmic imaging systems. *Biomed Opt Express*. 2021;12(4):2353–2372.
13. Mecê P, Gofas-Salas E, Rui Y, et al. Spatial-frequency-based image reconstruction to improve image contrast in multi-offset adaptive optics ophthalmoscopy. *Opt Lett*. 2021;46(5):1085–1088.
14. Sarna T, Burke JM, Korytowski W, et al. Loss of melanin from human RPE with aging: possible role of melanin photooxidation. *Exp Eye Res*. 2003;76(1):89–98.
15. Boulton M, Docchio F, Dayhaw-Barker P, Ramponi R, Cubeddu R. Age-related changes in the morphology, absorption and fluorescence of melanosomes and lipofuscin granules of the retinal pigment epithelium. *Vision Res*. 1990;30(9):1291–1303.
16. Bonilha VL, Bell BA, Hu J, et al. Geographic atrophy: confocal scanning laser ophthalmoscopy, histology, and inflammation in the region of expanding lesions. *Invest Ophthalmol Vis Sci*. 2020;61(8):15.
17. Pilotto E, Vujosevic S, Melis R, et al. Short wavelength fundus autofluorescence versus near-infrared fundus autofluorescence, with microperimetric correspondence, in patients with geographic atrophy due to age-related macular degeneration. *Br J Ophthalmol*. 2011;95(8):1140–1144.
18. Forte R, Querques G, Querques L, Massamba N, Le Tien V, Souied EH. Multimodal imaging of dry age-related macular degeneration. *Acta Ophthalmol (Copenh)*. 2012;90(4):e281–e287.
19. Heiferman MJ, Fawzi AA. Discordance between blue-light autofluorescence and near-infrared autofluorescence in age-related macular degeneration. *Retina Phila Pa*. 2016;36(Suppl 1):S137–S146.
20. Schmitz-Valckenberg S, Lara D, Nizari S, et al. Localisation and significance of in vivo near-infrared autofluorescent signal in retinal imaging. *Br J Ophthalmol*. 2011;95(8):1134–1139.
21. Paques M, Norberg N, Chaumette C, et al. Long term time-lapse imaging of geographic atrophy: a pilot study. *Front Med (Lausanne)*. 2022;9:868163.
22. Boretsky A, Khan F, Burnett G, et al. In vivo imaging of photoreceptor disruption associated with age-related macular degeneration: a pilot study. *Lasers Surg Med*. 2012;44(8):603–610.
23. Zayit-Soudry S, Duncan JL, Syed R, Menghini M, Roorda AJ. Cone structure imaged with adaptive optics scanning

laser ophthalmoscopy in eyes with nonneovascular age-related macular degeneration. *Invest Ophthalmol Vis Sci*. 2013;54(12):7498–7509.

24. Qin J, Rinella N, Zhang Q, et al. OCT angiography and cone photoreceptor imaging in geographic atrophy. *Invest Ophthalmol Vis Sci*. 2018;59(15):5985–5992.
25. Lazar R, Degen J, Fiechter AS, Monticelli A, Spitschan M. Regulation of pupil size in natural vision across the human lifespan. *R Soc Open Sci*. 2024;11(6):191613.
26. Guillon M, Dumbleton K, Theodoratos P, Gobbe M, Wooley CB, Moody K. The effects of age, refractive status, and luminance on pupil size. *Optom Vis Sci*. 2016;93(9):1093.
27. Kadlecová V, Peleška M, Vaško A. Dependence on age of the diameter of the pupil in the dark. *Nature*. 1958;182(4648):1520–1521.
28. Grieve K, Gofas-Salas E, Ferguson RD, Sahel JA, Paques M, Rossi EA. In vivo near-infrared autofluorescence imaging of retinal pigment epithelial cells with 757 nm excitation. *Biomed Opt Express*. 2018;9(12):5946–5961.
29. Murari J, Gautier J, Daout J, et al. Foveolar drusen decrease fixation stability in pre-symptomatic AMD. *Invest Ophthalmol Vis Sci*. 2024;65(8):13.
30. Penfold PL, Madigan MC, Gillies MC, Provis JM. Immunological and aetiological aspects of macular degeneration. *Prog Retin Eye Res*. 2001;20(3):385–414.
31. Augustin S, Lam M, Lavalette S, et al. Melanophages give rise to hyperreflective foci in AMD, a disease-progression marker. *J Neuroinflammation*. 2023;20:28.
32. Cao D, Leong B, Messinger JD, et al. Hyperreflective foci, optical coherence tomography progression indicators in age-related macular degeneration, include transdifferentiated retinal pigment epithelium. *Invest Ophthalmol Vis Sci*. 2021;62(10):34.
33. Midena E, Torresin T, Velotta E, Pilotto E, Parrozzani R, Frizziero L. OCT hyperreflective retinal foci in diabetic retinopathy: a semi-automatic detection comparative study. *Front Immunol*. 2021;12:613051.
34. Gofas-Salas E, Lee DMW, Rondeau C, et al. Comparison between two adaptive optics methods for imaging of individual retinal pigmented epithelial cells. *Diagn Basel Switz*. 2024;14(7):768.
35. Guillonneau X, Eandi CM, Paques M, Sahel JA, Sapieha P, Sennlaub F. On phagocytes and macular degeneration. *Prog Retin Eye Res*. 2017;61:98–128.
36. Zanzottera EC, Messinger JD, Ach T, Smith RT, Freund KB, Curcio CA. The project MACULA retinal pigment epithelium grading system for histology and optical coherence tomography in age-related macular degeneration. *Invest Ophthalmol Vis Sci*. 2015;56(5):3253–3268.
37. Curcio CA, Zanzottera EC, Ach T, Balaratnasingam C, Freund KB. Activated retinal pigment epithelium, an optical coherence tomography biomarker for progression in age-related macular degeneration. *Invest Ophthalmol Vis Sci*. 2017;58(6):BIO211–BIO226.
38. Guymer RH, Rosenfeld PJ, Curcio CA, et al. Incomplete retinal pigment epithelial and outer retinal atrophy in age-related macular degeneration: classification of Atrophy Meeting Report 4. *Ophthalmology*. 2020;127(3):394–409.
39. Laiginhas R, Liu J, Shen M, et al. Multimodal imaging, OCT B-scan localization, and en face OCT detection of macular hyperpigmentation in eyes with intermediate age-related macular degeneration. *Ophthalmol Sci*. 2022;2(2):100116.
40. Ortolan D, Sharma R, Volkov A, et al. Single-cell–resolution map of human retinal pigment epithelium helps discover subpopulations with differential disease sensitivity. *Proc Natl Acad Sci USA*. 2022;119(19):e2117553119.
41. Pedersen HR, Gilson S, Hagen LA, Holtan JP, Bragadottir R, Baraas RC. Multimodal in-vivo maps as a tool to characterize retinal structural biomarkers for progression in adult-onset Stargardt disease. *Front Ophthalmol (Lausanne)*. 2024;4:1384473.

Investigative Ophthalmology & Visual Science